

Resonant s -channel dark matter annihilation at NLO

M. Laine

*AEC, Institute for Theoretical Physics, University of Bern,
Sidlerstrasse 5, CH-3012 Bern, Switzerland*

Abstract

Studies of dark matter annihilation through an s -channel resonance are often based on recipes such as a narrow width approximation or real intermediate state subtraction. We review a recipe-free formalism that can be implemented at the NLO level in the full theory, and ensures the cancellation of mass singularities. Its basic ingredients can be formulated in the relativistic regime, but we show that the procedure simplifies if we go to the non-relativistic one and assume the presence of kinetic equilibrium. The latter case is illustrated for scalar singlet dark matter with $m_\varphi \simeq 60$ GeV, freezing out at $T \simeq (1 - 3)$ GeV, re-confirming the viability of this scenario with couplings tiny enough to evade experimental constraints.

Contents

1	Introduction	1
2	Boltzmann equation and how to go beyond it	3
2.1	Basic setup and one of its deficiencies	3
2.2	Maximal interaction rate	4
2.3	Chemical equilibration rate	6
3	Matrix elements squared	9
3.1	Overview	9
3.2	Model and parameters	9
3.3	Which processes are important?	10
4	Numerical results	11
5	Summary and outlook	13
A	Details of matrix elements squared	15
A.1	Gauge and scalar effects	16
A.2	Leptonic and hadronic effects	17
B	Phase space integrals for the leading-order process	17

1. Introduction

As traditional dark matter scenarios are put under pressure by collider searches and direct and indirect observational constraints, refined frameworks may become interesting. One possibility originates through “resonant” effects [1,2]. Notably, the resonance could originate via an attractive t -channel exchange of light force carriers, leading to a large enhancement in the spectral density of low-energy scattering states and possibly even to bound states between dark sector particles; or it could be an elementary excitation created in the s -channel, with a mass larger than twice the dark matter mass. Both of these could lead to an efficient depletion of dark matter particles in the early universe, whereby the correct abundance could be reached via the freeze-out mechanism, despite tiny couplings to the Standard Model.

To make the point concrete, we recall that among the simplest dark matter models is Standard Model extended by a singlet scalar field [3–6]. As this setup has been studied in increasing detail, a curious corner of parameter space has been identified, with a small singlet mass $m_\varphi \sim 60 \text{ GeV} < m_h/2$ and very weak couplings, which is not phenomenologically excluded, despite the weak-scale mass (cf., e.g., ref. [7] and references therein).

Curious corners of parameter space sometimes invoke non-trivial physics. Indeed, for the said example, a substantial argument has emerged between two groups [8–11], concerning the role that kinetic equilibrium plays in this scenario. This has led, amongst others, to recipes for treating kinetic non-equilibrium in a numerically more manageable manner [8–14].

However, apart from kinetic non-equilibrium, there could be other reasons for uncertainties in existing computations. One issue is that, as exemplified by ref. [6], the annihilation cross section of scalar singlet particles to Standard Model particles has been estimated by giving the Higgs propagator a finite width, namely its well-known vacuum decay rate. Though a reasonable approximation numerically, this is conceptually unsatisfactory, given that the Bose enhancement or Pauli blocking factors of the final-state particles in a thermal environment are omitted.¹ Indeed the Higgs width is known to be modified by thermal corrections [15]. Another problem is that dark matter freeze-out takes place in the temperature regime $T \sim (1 - 3)$ GeV, where poorly understood QCD effects could be substantial.

The purpose of the present paper is to address the latter uncertainties from a somewhat more general perspective, while not (yet) tackling the issue of kinetic non-equilibrium. The basic point is that in an unresummed order-by-order computation, an s -channel resonance is to be treated as an on-shell particle. The dominant dark matter annihilation channel is then the $2 \rightarrow 1$ “inverse decay” of two singlet scalars into an on-shell Higgs. The Higgs decays, represented by the width, are next-to-leading order (NLO) reactions, such as $2 \rightarrow 2$. However, at the same order, virtual corrections to the $2 \rightarrow 1$ process should be included, and are in fact crucial, as they cancel mass singularities according to the KLN theorem [17, 18]. By formulating the theoretical side by a consistent NLO treatment including these effects, we may also hope to incorporate thermal QCD effects in a somewhat reasonable manner.

Our presentation is organized as follows. Most dark matter computations adopt Boltzmann equations as their starting point. In sec. 2, we recall why text-book Boltzmann equations provide an incomplete treatment of nature when proceeding towards the NLO level, and one way to rectify them by a quantum-field theoretic computation. Moreover the simplifications met in the non-relativistic regime and in the presence of kinetic equilibrium are spelled out. In sec. 3, the ingredients needed for implementing the NLO treatment are summarized for the scalar singlet model, with details of matrix elements squared relegated to appendix A, and leading-order phase-space integrals to appendix B. Our numerical results are presented in sec. 4. We turn to a summary in sec. 5, adding at the same time a proposal on how the issue of kinetic non-equilibrium might be attacked beyond the Boltzmann level.

¹In vacuum, it has been proposed that this approximation can be systematized into an effective field theory [16], however its application to a general thermal environment is unclear, since the center-of-mass frame of the 2-particle final state differs from the plasma rest frame.

2. Boltzmann equation and how to go beyond it

2.1. Basic setup and one of its deficiencies

Denoting by $\mathcal{K} \equiv (\omega, \mathbf{k})$ the four-momentum of a dark matter particle, which is here assumed to be a boson of mass m_φ , so that $\omega \equiv \sqrt{k^2 + m_\varphi^2}$ where $k \equiv |\mathbf{k}|$; and by f_φ its phase space density, the Boltzmann equation governing the dark matter evolution has in local Minkowskian coordinates in the plasma rest frame the form

$$\mathcal{K}^\alpha \partial_\alpha f_\varphi = - \sum_{m,n} \text{aver}_{1+m \rightarrow n}(a_1, \dots, a_m; b_1, \dots, b_n) c \sum_{\text{spins}} |\mathcal{M}|_{\varphi+m \rightarrow n}^2, \quad (2.1)$$

where we have assumed the “mostly minus” metric convention; the a_i label particles in the initial state of the loss term (in addition to φ); the b_i stand for final-state particles in the loss term; and the phase space average has been defined as

$$\begin{aligned} \text{aver}_{1+m \rightarrow n}(a_1, \dots, a_m; b_1, \dots, b_n) &\equiv \frac{1}{2} \int d\Phi_{1+m \rightarrow n} \\ &\times \left\{ f_\varphi f_{a_1} \cdots f_{a_m} (1 \pm f_{b_1}) \cdots (1 \pm f_{b_n}) - f_{b_1} \cdots f_{b_n} (1 + f_\varphi) (1 \pm f_{a_1}) \cdots (1 \pm f_{a_m}) \right\}. \end{aligned} \quad (2.2)$$

The phase space integral goes over the momenta of the particle sets $\{a_i\}$ and $\{b_i\}$, and the signs \pm apply to bosons and fermions, respectively. The factor $c \equiv 1/(i_a! i_b!)$ in eq. (2.1) cancels overcounting when integrating over the momenta of i_a or i_b identical particles in the initial or final state. The sum \sum_{spins} in eq. (2.1) goes over polarizations, and we have assumed the symmetry $|\mathcal{M}|_{\varphi+m \rightarrow n}^2 = |\mathcal{M}|_{n \rightarrow \varphi+m}^2$ for the matrix elements squared.

In the following, we assume that all Standard Model particles are in thermal equilibrium, so that their phase space distribution f can be replaced by the Bose ($\equiv f_B$) or Fermi distribution ($\equiv f_F$). For equilibrated particles, $1 \pm f_a = e^{\beta \epsilon_a} f_a$, where $\beta \equiv 1/T$ and the momenta were written as $\mathcal{P}_a \equiv (\epsilon_a, \mathbf{p}_a)$. If the φ -particles were also in full equilibrium, then energy conservation, $\omega + \epsilon_{a_1} + \dots + \epsilon_{a_m} = \epsilon_{b_1} + \dots + \epsilon_{b_n}$, would guarantee detailed balance, i.e. that the right-hand side of eq. (2.2) vanishes.

In the physical situation, the φ -particles may fall out of chemical and/or kinetic equilibrium. Thereby eq. (2.1) turns into an integro-differential equation for f_φ . Even though such equations can be solved, by discretizing momentum space (and, if the system is not translationally invariant, configuration space as well), the solution tends to be numerically expensive. Furthermore, such a solution does *not* represent an exact treatment of nature.

To appreciate the latter point, we recall that one deficiency of the Boltzmann equation in eq. (2.1) is that its building blocks are what we call *real processes*, between on-shell particles whose phase-space distributions we know or want to determine. *Virtual corrections* (closed loops) can only be incorporated in so far as they amount to vacuum corrections to the matrix elements squared. But virtual corrections involving thermal effects — for instance,

thermal corrections to masses or couplings, or more generally thermal corrections to dispersion relations — are not present. Yet this can be important, for instance by opening up new channels that would not be allowed by vacuum kinematics.

It is for this reason that for a systematic treatment, the Boltzmann equation needs to be replaced by a quantum field theoretic description, in which both real and virtual processes, as well as all cancellations between them, are automatically present. It is not clear, *a priori*, how this can be achieved in general (though specific examples have been worked out, see e.g. ref. [19]). However, one transparent possibility is if we can define coefficients that amount to *equilibration rates*, which have an unambiguous physical meaning in the linear response regime. In the present paper, we show how this can be achieved through the definitions of a somewhat formal construction that we call the maximal interaction rate, and the physically important chemical equilibration rate, in secs. 2.2 and 2.3, respectively.

2.2. Maximal interaction rate

The purpose of the present section is to manipulate the Boltzmann equation in eq. (2.1) in order to identify what we term the maximal interaction rate. It should be stressed from the outset that the result is not inherent to a Boltzmann equation, but more general. In other words, the assumptions we make for its derivation are sufficient but not necessary. For instance, in ref. [20], the same rate and rate equation were obtained from quantum field theory, by carrying out an analysis to leading order in a weak coupling between a φ -field and Standard Model, but to all orders in Standard Model couplings.

Let us assume for a moment that f_φ is close to equilibrium, apart from around the momentum bin \mathbf{k} , and expand to first order in deviations in this bin, *viz.*

$$f_\varphi = \bar{f}_\varphi + \delta f_\varphi, \quad \bar{f}_\varphi(k) \equiv f_B(\omega), \quad \delta f_\varphi(k) \equiv f_\varphi(k) - f_B(\omega). \quad (2.3)$$

Given that a single momentum bin can be excluded from the integrations over \mathcal{P}_{a_i} and \mathcal{P}_{b_i} in eq. (2.2) without significantly affecting the outcome, f_φ can be replaced by f_B if it appears in the sets $\{a_i\}$ or $\{b_i\}$. Recalling furthermore that the zeroth order term vanishes by detailed balance, it follows from eq. (2.2) that, to first order in δf_φ ,

$$\begin{aligned} & \text{aver}_{1+m \rightarrow n}(a_1, \dots, a_m; b_1, \dots, b_n) \\ &= \delta f_\varphi \times \frac{1}{2} \int d\Phi_{1+m \rightarrow n} \left\{ f_{\sigma_{a_1}} \cdots f_{\sigma_{a_m}} (1 + f_{\sigma_{b_1}}) \cdots (1 + f_{\sigma_{b_n}}) \right. \\ & \quad \left. - f_{\sigma_{b_1}} \cdots f_{\sigma_{b_n}} (1 + f_{\sigma_{a_1}}) \cdots (1 + f_{\sigma_{a_m}}) \right\} (-1)^F + \mathcal{O}(\delta f_\varphi^2) \\ &\equiv [f_\varphi(k) - f_B(\omega)] \times \text{scat}_{1+m \rightarrow n}(-a_1, \dots, -a_m; b_1, \dots, b_n) (-1)^F + \mathcal{O}(\delta f_\varphi^2). \end{aligned} \quad (2.4)$$

Here $\sigma_i = \pm$ denotes the statistics of each particle species; we have introduced $f_+ \equiv f_B$, $f_- \equiv -f_B$; F is the number of fermions in the initial (or final) state; $(-1)^F$ is a factor

originating from the sign difference between f_- and f_+ ; and $\text{scat}_{1+m \rightarrow n}$ corresponds to the notation introduced in ref. [21].

The rationale for introducing negative signs in front of the particle labels in the argument of $\text{scat}_{1+m \rightarrow n}$ in eq. (2.4) is that $\text{scat}_{1+m \rightarrow n}$ can be defined as an operator, such that negative labels invert the signs of the corresponding momenta in the matrix element squared. Thereby all matrix elements squared can be obtained by crossings from a would-be decay matrix element squared, which enjoys maximal symmetries. Specifically, defining

$$\Theta(\mathcal{P}_{a_1}, \dots, \mathcal{P}_{a_m}, \mathcal{P}_{b_1}, \dots, \mathcal{P}_{b_n}) \equiv c \sum_{\text{spins}} |\mathcal{M}|_{\varphi \rightarrow m+n}^2, \quad (2.5)$$

where all momenta are now in the final state, the combination originating from eqs. (2.1) and (2.4) amounts to

$$(-1)^F c \sum_{\text{spins}} |\mathcal{M}|_{\varphi+m \rightarrow n}^2 = \Theta(-\mathcal{P}_{a_1}, \dots, -\mathcal{P}_{a_m}, \mathcal{P}_{b_1}, \dots, \mathcal{P}_{b_n}). \quad (2.6)$$

Adopting the operator notation, we define the real-scattering part of an interaction rate as

$$\omega \Gamma_{\text{max}}^{\text{real}}(k) \equiv \sum_{m,n} \text{scat}_{1+m \rightarrow n}(-a_1, \dots, -a_m; b_1, \dots, b_n) \Theta(\mathcal{P}_{a_1}, \dots, \mathcal{P}_{a_m}, \mathcal{P}_{b_1}, \dots, \mathcal{P}_{b_n}). \quad (2.7)$$

Now, if eq. (2.7) originates from a quantum field theoretic equilibration rate, in the sense described in ref. [20], where it corresponds to the imaginary part of a retarded self-energy, then the full rate includes also *virtual processes*. We denote the latter by $\Gamma_{\text{max}}^{\text{virt}}$. At NLO, the physical, and thereby ultraviolet (UV) and infrared (IR) finite rate, is given by

$$\Gamma_{\text{max}}^{\text{phys}}(k) = \Gamma_{\text{max}}^{\text{real}}(k) + \Gamma_{\text{max}}^{\text{virt}}(k). \quad (2.8)$$

Going over to an expanding background, with the Hubble rate denoted by $H \equiv \dot{a}/a$, and assuming furthermore that f_φ is translationally invariant, eq. (2.1) then takes the form

$$(\partial_t - Hk \partial_k) f_\varphi(k) = -\Gamma_{\text{max}}^{\text{phys}}(k) [f_\varphi(k) - f_{\text{B}}(\omega)] + \mathcal{O}(\delta f_\varphi^2). \quad (2.9)$$

This equation can be viewed as describing equilibration in the sense of linear response theory. On the other hand, by setting $f_\varphi \rightarrow 0$ on the right-hand side, it defines the production rate of the φ particles from a plasma. Both interpretations underline that the equation has a physical meaning beyond Boltzmann equations.

A cautionary word needs to be added, however. Even though eq. (2.9) shows that $\Gamma_{\text{max}}^{\text{phys}}$ drives the system towards the Bose distribution if the system is already close to it, $\Gamma_{\text{max}}^{\text{phys}}$ should *not* be interpreted as a kinetic equilibration rate. Indeed kinetic equilibration is a notion associated with particles whose phase-space distribution can differ from equilibrium by an overall factor (if the particles are out of chemical equilibrium) and by a different shape.

Kinetic equilibration involves transfer of momentum, in order to rectify the shape, but the overall normalization should not be simultaneously changed, as it represents the number density. Instead, eq. (2.9) represents the maximal rate at which the φ -particles interact; apart from a change of momentum or particle number, this includes the very fast processes that lead to phase decoherence in quantum mechanics.

2.3. Chemical equilibration rate

In the previous section we defined a rate from Boltzmann equations which can arguably be generalized to have a quantum field theoretic meaning, as the imaginary part of a retarded self-energy in the linear response regime. We start the present section by recalling that in the non-relativistic limit such rates have a well-defined subpart, which then also has a quantum field theoretic meaning. Subsequently, returning to Boltzmann equations, we show that the momentum average of this subpart has an interpretation as the chemical equilibration rate.²

Let us separate all possible scatterings into two classes, according to whether the number of φ particles changes in the reaction (“inelastic processes”), or not (“elastic processes”), *viz.*

$$\Gamma_{\text{max}}^{\text{phys}}(k) \equiv \Gamma_{\text{inel}}^{\text{phys}}(k) + \Gamma_{\text{elas}}^{\text{phys}}(k) . \quad (2.10)$$

The same division can be made separately in $\Gamma_{\text{max}}^{\text{real}}$ and $\Gamma_{\text{max}}^{\text{virt}}$. In some theories all reactions are inelastic, but the division is non-trivial if the system displays a global or discrete symmetry, as is typically the case in dark matter models. It is sufficient if the symmetry is an approximate one, emerging for instance in the non-relativistic limit.

The inelastic and elastic processes proceed with very different rates if $T \ll m_\varphi$. In this situation $\Gamma_{\text{inel}}^{\text{phys}}$ is exponentially suppressed compared with $\Gamma_{\text{elas}}^{\text{phys}}$, *viz.*

$$\Gamma_{\text{inel}}^{\text{phys}} \sim e^{-m_\varphi/T} \Gamma_{\text{elas}}^{\text{phys}} , \quad T \ll m_\varphi . \quad (2.11)$$

The reason is the appearance of an additional φ particle in the initial or final state.

If the hierarchy in eq. (2.11) is present, there is a temperature regime in which the system should be in kinetic equilibrium, but out of the chemical one. To describe such a system, we may take a momentum average, and adopt $n_\varphi \equiv \int_{\mathbf{k}} f_\varphi$ as the only non-equilibrium variable.

To obtain an equation for n_φ , we return to eq. (2.1), assume f_φ to be translationally invariant, and divide by ω . Working in an expanding background, the integral over \mathbf{k} yields $(\partial_t + 3H)n_\varphi$ on the left-hand side. A key point is that on the right-hand side, the division by ω and the integration over \mathbf{k} imply that the matrix element squared is averaged over *all momenta*. Then we can symmetrize the average. In particular, for processes leading to the

²In the non-relativistic limit a chemical equilibration rate can also be defined directly in quantum field theory [22], with the connection to Boltzmann equations then following in the course of its practical evaluation.

elastic part of eq. (2.10), we can exchange initial- and final-state momenta, symbolically as

$$\begin{aligned}
& \int_{\mathbf{k}} \frac{1}{2\omega} \int d\Phi_{1+m \rightarrow n} \{ f_{\varphi}(1 + f_{b_{1\varphi}}) \times f_{a_1} \cdots f_{a_m}(1 \pm f_{b_2}) \cdots (1 \pm f_{b_n}) \\
& - (1 + f_{\varphi})f_{b_{1\varphi}} \times f_{b_2} \cdots f_{b_n}(1 \pm f_{a_1}) \cdots (1 \pm f_{a_m}) \} \\
& \stackrel{\varphi \leftrightarrow b_{1\varphi}}{=} \int_{a_1 \cdots a_m \leftrightarrow b_2 \cdots b_n} \int_{\mathbf{k}} \frac{1}{2\omega} \int d\Phi_{1+m \rightarrow n} \{ f_{b_{1\varphi}}(1 + f_{\varphi}) \times f_{b_2} \cdots f_{b_n}(1 \pm f_{a_1}) \cdots (1 \pm f_{a_m}) \\
& - (1 + f_{b_{1\varphi}})f_{\varphi} \times f_{a_1} \cdots f_{a_m}(1 \pm f_{b_2}) \cdots (1 \pm f_{b_n}) \} .
\end{aligned} \tag{2.12}$$

The two terms are opposites of each other, and the result cancels by antisymmetry. If the number of spectators changes, there are two different processes (spectators increase or decrease), each with their own loss and gain terms. Then we may inspect the four processes together, and the substitution $\varphi \leftrightarrow b_{1\varphi}$ alone shows that elastic processes drop out.³

For the inelastic processes, the left-hand side of eq. (2.12) is replaced with (we show this with the example of two dark matter particles in the initial and none in the final state, however this can be generalized, see below)

$$\begin{aligned}
& \int_{\mathbf{k}} \frac{1}{2\omega} \int d\Phi_{1+m \rightarrow n} \{ f_{\varphi}f_{a_{1\varphi}} \times f_{a_2} \cdots f_{a_m}(1 \pm f_{b_1}) \cdots (1 \pm f_{b_n}) \\
& - (1 + f_{\varphi})(1 + f_{a_{1\varphi}}) \times f_{b_1} \cdots f_{b_n}(1 \pm f_{a_2}) \cdots (1 \pm f_{a_m}) \} .
\end{aligned} \tag{2.13}$$

Let us analyze this in the linear response regime, writing $f_{\varphi} \rightarrow \bar{f}_{\varphi} + \delta f_{\varphi}$. Then

$$f_{\varphi}f_{a_{1\varphi}} \rightarrow \underbrace{\bar{f}_{\varphi}\bar{f}_{a_{1\varphi}}}_{\text{cancels by detailed balance}} + \underbrace{\delta f_{\varphi}\bar{f}_{a_{1\varphi}} + \bar{f}_{\varphi}\delta f_{a_{1\varphi}}}_{\varphi \leftrightarrow a_{1\varphi} \Rightarrow 2\delta f_{\varphi}\bar{f}_{a_{1\varphi}}} + \mathcal{O}(\delta^2) , \tag{2.14}$$

$$\begin{aligned}
(1 + f_{\varphi})(1 + f_{a_{1\varphi}}) & \rightarrow \underbrace{(1 + \bar{f}_{\varphi})(1 + \bar{f}_{a_{1\varphi}})}_{\text{cancels by detailed balance}} + \underbrace{\delta f_{\varphi}(1 + \bar{f}_{a_{1\varphi}}) + (1 + \bar{f}_{\varphi})\delta f_{a_{1\varphi}}}_{\varphi \leftrightarrow a_{1\varphi} \Rightarrow 2\delta f_{\varphi}(1 + \bar{f}_{a_{1\varphi}})} + \mathcal{O}(\delta^2) .
\end{aligned} \tag{2.15}$$

In total we get

$$(\partial_t + 3H)n_{\varphi} \approx - \sum_{m,n} \int_{\mathbf{k}} \frac{2\delta f_{\varphi}}{\omega} \frac{1}{2} \int d\Phi_{1+m \rightarrow n} \tag{2.16}$$

$$\begin{aligned}
& \times \{ \bar{f}_{a_{1\varphi}} \cdots f_{a_m}(1 \pm f_{b_1}) \cdots (1 \pm f_{b_n}) - f_{b_1} \cdots f_{b_n}(1 + \bar{f}_{a_{1\varphi}}) \cdots (1 \pm f_{a_m}) \} c \sum_{\text{spins}} |\mathcal{M}|_{\varphi+m \rightarrow n}^2 \\
& = -2 \int_{\mathbf{k}} \frac{\delta f_{\varphi}}{\omega} \omega \Gamma_{\text{max,inel}}^{\text{real}}(k) ,
\end{aligned} \tag{2.17}$$

³As already mentioned, we assume $c \sum_{\text{spins}} |\mathcal{M}|_{\varphi+m \rightarrow n}^2$ to be invariant in these exchanges.

where we recognized an inelastic part of the maximal interaction rate, defined in eq. (2.7).

Given that $\Gamma_{\text{max,inel}}^{\text{real}}$ is a well-defined subpart of $\Gamma_{\text{max}}^{\text{real}}$, we can consider the equally well-defined virtual correction $\Gamma_{\text{max,inel}}^{\text{virt}}$. At NLO, their sum yields

$$\Gamma_{\text{inel}}^{\text{phys}}(k) \equiv \Gamma_{\text{max,inel}}^{\text{real}}(k) + \Gamma_{\text{max,inel}}^{\text{virt}}(k) , \quad (2.18)$$

in analogy with eq. (2.8).

We may now generalize the consideration of eqs. (2.13)–(2.17). For a set of i dark matter particles appearing on one side only, we may undertake a symmetrization like in eqs. (2.14) and (2.15). Then we may represent $\Gamma_{\text{inel}}^{\text{phys}}(k)$ as

$$\Gamma_{\text{inel}}^{\text{phys}}(k) = \sum_{i=1}^{\infty} \Gamma_{\text{inel}(i)}^{\text{phys}}(k) . \quad (2.19)$$

Because of the symmetrization, the rate equation (2.22) obtains a symmetry factor i .

Finally, returning to eq. (2.17) and assuming kinetic equilibrium, the deviation of the phase-space density can be expressed as

$$\delta f_{\varphi}(k) = f_{\text{B}}(\omega) \frac{\delta n_{\varphi}}{n_{\text{eq}}} , \quad n_{\text{eq}} \equiv \int_{\mathbf{k}} f_{\text{B}}(\omega) , \quad \delta n_{\varphi} \equiv n_{\varphi} - n_{\text{eq}} . \quad (2.20)$$

The weighting by $f_{\text{B}}(\omega)$ and the division by n_{eq} in eq. (2.20) prompt us to define

$$\langle \Gamma_{\text{inel}(i)}^{\text{phys}} \rangle \equiv \frac{\int_{\mathbf{k}} \Gamma_{\text{inel}(i)}^{\text{phys}}(k) f_{\text{B}}(\omega)}{\int_{\mathbf{k}} f_{\text{B}}(\omega)} . \quad (2.21)$$

Thereby the momentum-averaged equation, expanded to first order in δn_{φ} , turns into

$$(\partial_t + 3H)n_{\varphi} = - \sum_{i=1}^{\infty} i \langle \Gamma_{\text{inel}(i)}^{\text{phys}} \rangle \delta n_{\varphi} + \mathcal{O}(\delta n_{\varphi}^2) . \quad (2.22)$$

In models with a discrete or continuous symmetry, the leading contribution originates from $i = 2$, and making use of $n_{\varphi} - n_{\text{eq}} \approx (n_{\varphi}^2 - n_{\text{eq}}^2)/(2n_{\text{eq}})$ as is valid in the linear response regime on which our derivation relied, we find the usual evolution equation,

$$(\partial_t + 3H)n_{\varphi} \approx -\langle \sigma v_{\text{rel}} \rangle (n_{\varphi}^2 - n_{\text{eq}}^2) , \quad \langle \sigma v_{\text{rel}} \rangle \equiv \frac{\langle \Gamma_{\text{inel}(2)}^{\text{phys}} \rangle}{n_{\text{eq}}} = \frac{\int_{\mathbf{k}} \Gamma_{\text{inel}(2)}^{\text{phys}} f_{\text{B}}}{n_{\text{eq}}^2} . \quad (2.23)$$

To summarize this section, we have argued that eq. (2.7) contains a part, namely processes that can be characterized as inelastic, cf. eq. (2.10), whose momentum average permits to define a chemical equilibration rate and a corresponding Boltzmann equation, cf. eq. (2.22). The strength of this formulation is that we can promote the rate coefficients to include virtual corrections, according to eq. (2.8), which ensures the absence of mass singularities [17,18]. In the linear response regime and assuming the presence of kinetic equilibrium, the formalism reduces to the usual form, cf. eq. (2.23). The coefficient $\langle \sigma v_{\text{rel}} \rangle$ incorporates the influence of fast processes, the functional form of eq. (2.23) those of the slow variables. Thereby eq. (2.23) can normally also be applied once freeze-out has taken place, i.e. $n_{\varphi} \gg n_{\text{eq}}$ [23].

3. Matrix elements squared

3.1. Overview

We have argued in the previous section that the dynamical information entering the dark matter evolution equation, cf. eq. (2.23), can be obtained from a general class of thermally averaged rates, cf. eq. (2.7), by restricting to inelastic processes and adding virtual corrections. For the class of eq. (2.7), an algorithm has been worked out in which all relevant channels, and the virtual corrections that cancel mass singularities, can be derived from minimal information, contained in the decay matrix elements defined in eq. (2.5) [21]. In this section, we illustrate how the procedure works, by introducing a specific model (cf. sec. 3.2).

As far as the notation goes, we employ thermal averages like in eq. (2.4), specifically $\text{scat}_{1 \rightarrow n}(b_1, \dots, b_n)$. Kinematic invariants are defined in the usual way,

$$s_{ij} \equiv (\mathcal{P}_{b_i} + \mathcal{P}_{b_j})^2. \quad (3.1)$$

For deriving matrix elements in which one φ is in the initial state and the rest of them appear in the final state, it is convenient to shift $\varphi \rightarrow \varphi + \tilde{\varphi}$ in the Lagrangian, and treat $\tilde{\varphi}$ as a thermalized final-state field. This simplifies the computation of combinatorial factors, and makes explicit the linear response philosophy.

3.2. Model and parameters

We illustrate the procedure of sec. 2 with the scalar singlet extension of the Standard Model (cf., e.g., refs. [3–6] and references therein), defined by

$$\mathcal{L} = \mathcal{L}_{SM} + \left\{ \frac{1}{2} \partial^\mu \varphi \partial_\mu \varphi - \left[\frac{1}{2} m_{\varphi 0}^2 \varphi^2 + \frac{1}{2} \kappa \varphi^2 H^\dagger H + \frac{1}{4} \lambda_\varphi \varphi^4 \right] \right\}, \quad (3.2)$$

where H is the Higgs doublet and an *ad hoc* $\mathbb{Z}(2)$ symmetry has been imposed in order to reduce the number of parameters. After electroweak symmetry breaking, the Higgs doublet is parametrized as

$$H = \frac{1}{\sqrt{2}} \begin{pmatrix} \phi_2 + i\phi_1 \\ v + h - i\phi_3 \end{pmatrix}, \quad (3.3)$$

where $v|_{T=0} \simeq 246$ GeV, h denotes the physical Higgs field, and the Goldstone modes ϕ_a are numbered in analogy with the Pauli matrices. The scalar singlet is assumed to be in its unbroken phase throughout the cosmic history, i.e. $m_{\varphi 0}^2 > 0$, and its tree-level vacuum mass is given by $m_\varphi^2 = m_{\varphi 0}^2 + \kappa v^2/2$.⁴

⁴At high temperatures, the singlet mass squared experiences thermal corrections, first of all due to $v^2|_T$, but also due to other effects, if $\pi T \gg \min\{m_\varphi, m_h\}$. However, since we assume coupling strengths such that freeze-out takes place deep in the non-relativistic regime, with $\pi T \ll \min\{m_\varphi, m_h\}$, these are unimportant for us and omitted for simplicity. If the vacuum value of m_φ were precisely known, however, even small effects could have an impact, due to the vicinity of the kinematic threshold at $m_\varphi \simeq m_h/2$.

On the Standard Model side, an important role is played by the charm and bottom quarks and the strong gauge coupling. The values of the charm and bottom masses are conventionally tabulated at a renormalization scale $\bar{\mu} \simeq 2 \text{ GeV}$, and we evolve them to a thermal scale $\bar{\mu} \simeq 2\pi T$. In addition, we scale the quark masses by the temperature dependence of the Higgs expectation value, $v|_T \simeq v|_0 \text{Re} \sqrt{1 - T^2/T_c^2}$, where the pseudocritical temperature $T_c \approx 160 \text{ GeV}$ can be adopted from ref. [24]. Of course, at the temperatures $T \sim (1 - 3) \text{ GeV}$ that are most important for us, the latter effect is minuscule.

As far as the top quark is concerned, it can be integrated out deep in the Higgs phase, which yields the effective operator [25]

$$\mathcal{L} \supset -\frac{g_3^2}{(4\pi)^2} \frac{h G_{\mu\nu}^a G^{a\mu\nu}}{3v}, \quad (3.4)$$

where $g_3^2 \equiv 4\pi\alpha_s$ is the strong gauge coupling and $G_{\mu\nu}^a$ is the SU(3) field strength tensor. We fix $\alpha_s(m_Z) \approx 0.118$, and again evolve this to $\bar{\mu} \simeq 2\pi T$. The role that eq. (3.4) plays for Higgs physics at temperatures of a few GeV has been elaborated upon in ref. [15].

For reference, let us start by briefly considering $T > 160 \text{ GeV}$, where electroweak symmetry is restored, *viz.* $v|_T \simeq 0$. This regime may play a role for freeze-in dark matter production, and also offers for a partial crosscheck of matrix elements squared, by their continuity. A relatively straightforward computation yields

$$\omega \Gamma_{1 \rightarrow 3}^{\text{real}} = 2\kappa^2 \text{scat}_{1 \rightarrow 3}(\tilde{\varphi}, \phi, \phi) + 6\lambda_\varphi^2 \text{scat}_{1 \rightarrow 3}(\tilde{\varphi}, \tilde{\varphi}, \tilde{\varphi}), \quad (3.5)$$

where the first term represents equilibration through Higgs scatterings, and the latter through φ self-interactions. By ϕ we have denoted a Standard Model scalar particle (with 4 real degrees of freedom) in the absence of electroweak symmetry breaking. As stressed before, even if the $1 \rightarrow 3$ decays in eq. (3.5) are kinematically forbidden, their algebraic forms capture the matrix elements squared of all allowed crossed channels. When we go to the Higgs phase, eq. (3.5) is replaced by an expression containing contributions from many channels, and we now turn to which of them are the most important ones.

3.3. Which processes are important?

When $T < 160 \text{ GeV}$, the Higgs mechanism is active. Then eq. (3.5) splits into many individual processes, and it is furthermore supplemented by additional matrix elements squared, proportional to v . The corresponding amplitudes are illustrated in fig. 1. The expressions are collected in appendix A, and here we single out the crucial ones.

We note, first of all, that in the temperature range of interest, $T \lesssim 10 \text{ GeV}$, many Standard Model particles are heavy ($m_{h, Z^0, W^\pm, t} \gg \pi T$). *Real processes* containing such external states are exponentially suppressed. At the same time, *virtual processes* involving these particles are not small: they contain large logarithms. But they are small compared with the $1 \leftrightarrow 2$

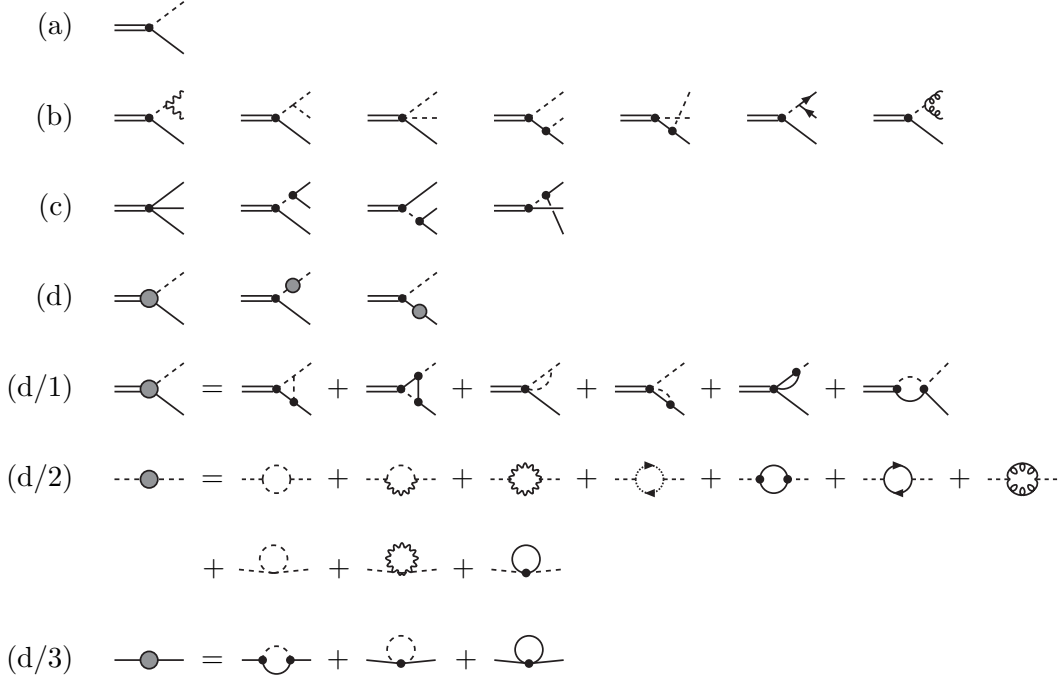


Figure 1: Amplitudes for the decay and/or production of a φ -particle (denoted by a double line). Many of these processes are kinematically forbidden, but this is inessential, as we only use them for extracting matrix elements squared; crossings lead to allowed processes, e.g. $2 \leftrightarrow 2$ scatterings, or $1 \leftrightarrow 2$ decays or inverse decays between a Higgs boson and two φ -particles. Dashed lines denote Higgs fields, wiggly lines weak gauge bosons, arrowed lines fermions, curly lines gluons, and straight lines thermalized singlet modes, denoted by $\tilde{\varphi}$ in sec. 3. Only physical particles (no Goldstones) are shown as final states. The small blobs denote non-Standard Model couplings, and the gray blobs virtual corrections. The amplitudes have been classified as: (a) $1 \rightarrow 2$ processes; (b) $1 \rightarrow 3$ processes with two singlets; (c) $1 \rightarrow 3$ processes with four singlets; (d) virtual corrections to $1 \rightarrow 2$ processes.

process, whose parameters they correct. As a leftover from correcting parameters, they also lead to higher-dimensional operators, the largest of which was introduced in eq. (3.4).

To summarize, the most important processes at $T \lesssim 10$ GeV are the leading-order $1 \leftrightarrow 2$ one; those $2 \leftrightarrow 2$ processes which contain particles with a mass $\lesssim \pi T$, like charm and bottom quarks, as these are not exponentially suppressed; as well as $2 \leftrightarrow 2$ processes originating through the higher-dimensional operator in eq. (3.4).

4. Numerical results

Given the matrix elements squared from appendix A, the algorithm of ref. [21] determines all crossed processes (specifically the $2 \rightarrow 2$ and $3 \rightarrow 1$ ones) contributing to the full rate

in eq. (2.7), as well as IR sensitive virtual corrections. According to eqs. (2.10) and (2.22), we subsequently select the inelastic reactions. Given that this subclass differs parameterically from the elastic processes, by $\sim e^{-m_\varphi/T}$, the cancellation of mass singularities remains guaranteed. After the inclusion of the virtual corrections, we obtain the coefficients denoted by $\Gamma_{\text{inel}}^{\text{phys}}$ in eq. (2.10). For simplicity we drop the superscript from the rate coefficients, employing from now on just Γ_{inel} .

On the side of technical details, we remark that second order poles in matrix elements squared are treated as parametric derivatives of first order poles, and first order poles are regularized as principal values. The dependence on the regularization drops out when real and virtual corrections are summed together. As for UV divergences in the virtual corrections, they are related to the renormalization of the parameters appearing in the $1 \leftrightarrow 2$ process. As already mentioned, a convenient choice is to set the renormalization scale to $\bar{\mu} \simeq 2\pi T$. In practice, choices related to renormalization are numerically insignificant in our example.

In order to model confining effects influencing charm and bottom quarks as well as gluons, we have adopted the phenomenological replacement $N_c \rightarrow N_{c,\text{eff}} < 3$ from ref. [26]. However, we have also considered the non-interacting value $N_c = 3$, and indicate the difference of the two prescriptions as an error band in fig. 2.

As for the parameters, the key choice is the value of the coupling κ in eq. (3.2). We have varied it around the value leading to the correct dark matter abundance, found to be

$$\kappa_{\text{dm[here]}} \approx 0.00064 \quad (m_\varphi \approx 60 \text{ GeV}) . \quad (4.1)$$

This is close to but slightly smaller than the values cited in refs. [8, 11] if kinetic equilibrium is assumed, $\kappa_{\text{dm[8]}} \simeq 0.00066$ and $\kappa_{\text{dm[11]}} \simeq 0.00068$, respectively.⁵

In fig. 2(left) different contributions to the absolute value of $\langle \Gamma_{\text{inel}(2)} \rangle$ are plotted, normalized to the Hubble rate. The plot shows that freeze-out must happen in the range $T \lesssim 2 \text{ GeV}$, when $\langle \Gamma_{\text{inel}(2)} \rangle \lesssim H$, and that NLO corrections are very small. To view the NLO corrections more clearly, we replot them in fig. 2(right) in the combination $\langle \sigma v_{\text{rel}} \rangle s / H = \langle \Gamma_{\text{inel}(2)} \rangle s / (n_{\text{eq}} H)$, where s is the entropy density.

Given the value of $\langle \sigma v_{\text{rel}} \rangle s / H$ from fig. 2(right), we can integrate eq. (2.23). In practice, it is convenient to normalize number densities by the entropy density s , denoting the corresponding yield parameters by $Y_\varphi \equiv n_\varphi / s$, $Y_{\text{eq}} \equiv n_{\text{eq}} / s$. Introducing $x \equiv \ln(T_{\text{max}}/T)$ as an integration variable, and making use of the Jacobian $dx/dt = 3c_s^2 H$, where $c_s^2 = \partial p / \partial e$ is the speed of sound squared, eq. (2.23) turns into

$$\partial_x Y_\varphi \approx - \frac{\langle \sigma v_{\text{rel}} \rangle s}{3c_s^2 H} (Y_\varphi^2 - Y_{\text{eq}}^2) . \quad (4.2)$$

⁵The much larger couplings also discussed in ref. [8] correspond to their case ‘B’ that omits the elastic channels involving charm and bottom quarks, so that the system is far from kinetic equilibrium.

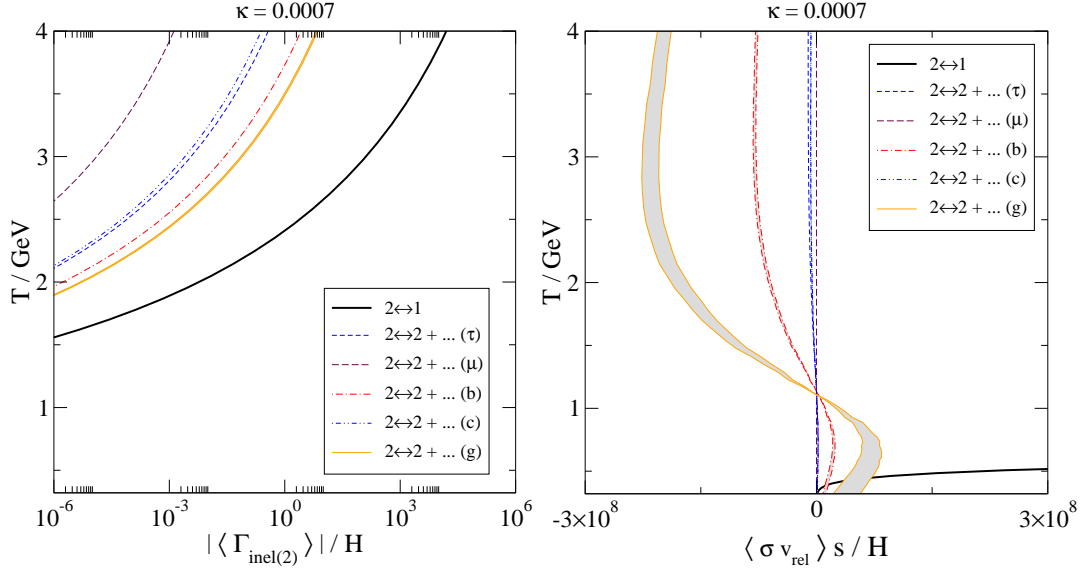


Figure 2: Left: the absolute value of the momentum-averaged chemical equilibration rate from eq. (2.21), separated into contributions from different channels, with “+...” indicating virtual corrections. Freeze-out starts when $\langle \Gamma_{\text{inel}(2)} \rangle \sim H$, and in this regime NLO corrections are suppressed by orders of magnitude with respect to the $2 \leftrightarrow 1$ channel. Right: the coefficient $\langle \sigma v_{\text{rel}} \rangle$ from eq. (2.23), normalized as it appears in eq. (4.2) (the factor $3c_s^2 \simeq 1$ has been omitted here, though it is included in our solution). The purpose of this figure is to illustrate that NLO corrections can be negative, because of their virtual part, and because the real part involves a principal value integral or its derivative, however this only happens in a regime where the NLO corrections are utterly subdominant. The grey bands indicate uncertainties in the evaluation of hadronic contributions.

For the thermodynamic functions s and c_s^2 we adopt values derived in refs. [27, 28].⁶ From Y_φ , the current energy density follows as $\Omega_\varphi/\Omega_{\text{dm}} \approx 2.29 (m_\varphi/\text{eV}) Y_\varphi(x_{\text{today}})$, where $\Omega_{\text{dm}} h^2 \approx 0.120$ refers to the observed value and h is the reduced Hubble rate. The results obtained with the benchmark value $m_\varphi \simeq 60$ GeV, both for Y_φ and $\Omega_\varphi/\Omega_{\text{dm}}$, are shown in fig. 3.

5. Summary and outlook

The common tool of dark matter computations, Boltzmann equations in their text-book form, do not incorporate thermal virtual corrections (i.e. closed loops involving Bose and/or Fermi distributions), even though such effects could be important. On the formal level, they are necessary for cancelling mass singularities (mass thresholds or massless limits) that originate from real scatterings. Physically, they lead to modified dispersion relations, and could then open up or close specific annihilation channels.

⁶These are tabulated at the web site <http://www.laine.itp.unibe.ch/eos15/>.

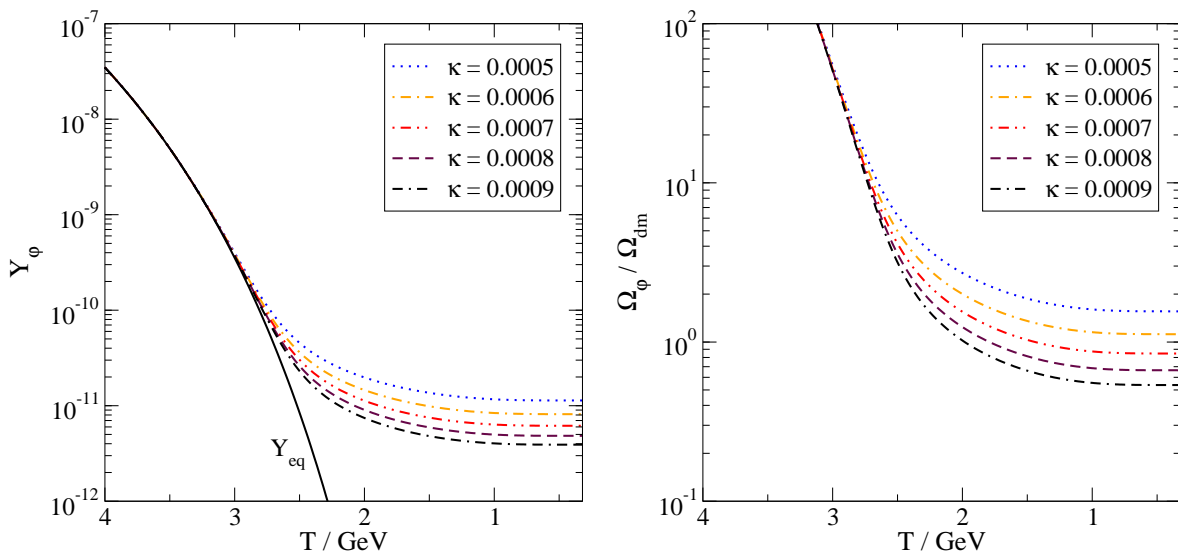


Figure 3: Left: the solution of eq. (4.2) for a few values of κ , keeping the scalar singlet mass fixed at $m_\varphi \simeq 60$ GeV. Right: the same for the fractional contribution of φ to the dark matter energy density. The hadronic error bands from fig. 2 are much narrower than the line widths, given that hadronic effects are much suppressed compared with the $2 \leftrightarrow 1$ process when $T = (1 - 3)$ GeV.

The purpose of this paper has been to illustrate a way to include thermal virtual corrections when dark matter annihilation is influenced by an s -channel resonance. The treatment is simple-minded, both conceptually and technically. As a first step we carry out a systematic perturbative determination of the imaginary part of a retarded self-energy in the linear response regime,⁷ treating the narrow resonance as an on-shell particle at leading order. We found that a convenient way to implement this computation is the substitution $\varphi \rightarrow \varphi + \tilde{\varphi}$, explained in sec. 3.1. The finite width of the Higgs boson, modified by thermal corrections from Bose enhancement or Pauli blocking, originates as a part of NLO corrections, notably $2 \leftrightarrow 2$ scatterings. But the finite width is not the only NLO correction: virtual corrections to the leading-order $2 \leftrightarrow 1$ process are of the same order and included at the same time.

If the physics that we are interested in takes place in the non-relativistic regime, and kinetic equilibrium can be assumed, the procedure can be completed by a second step. From the imaginary part of the retarded self-energy, we may identify the subpart that originates from inelastic reactions, and consider its momentum average. We have shown that this reproduces the standard notion of the chemical equilibration rate (cf. sec. 2.3), and ultimately leads to the usual cosmological evolution equation (cf. eq. (2.23)). However, the overall philosophy should apply more generally than to systems in kinetic equilibrium, notably to freeze-in scenarios

⁷In particular, resummations have not been touched upon, even though they could become important if we go very close to the resonance production threshold.

that operate in the relativistic or ultrarelativistic regime (cf., e.g., refs. [14, 29]), even if the practical implementation to such cases requires further consideration.

For an illustration, we returned to the well-studied example of scalar singlet dark matter, assuming again that kinetic equilibrium is maintained by elastic scatterings. Then all NLO corrections are small (cf. fig. 2), and the thermally averaged cross section can be computed analytically (cf. eq. (B.7)). Numerically, these results are in good agreement with previous literature (cf. sec. 4), which relied on more complicated computations.

Finally, in view of intensive discussions of the topic [8–13], we would like to put forward one possibility for investigating kinetic non-equilibrium in the non-relativistic regime. This is the use of Langevin simulations for determining momentum distributions. The Langevin description assumes that kinetic equilibrium is established by elastic scatterings and that the corresponding scattering rate is much smaller than the typical plasma interaction rates, i.e. that the dark matter particles are weakly coupled. But it does *not* assume that the plasma particles are weakly coupled among themselves. Therefore it permits for the inclusion of NLO [30] or even non-perturbative information on the plasma interactions [31], as is certainly desirable for strongly interacting particles at $T \simeq (1-3)$ GeV. We note that such frameworks have been widely applied for understanding the kinetic equilibration of charm and bottom quarks in the heavy ion collision context [32].

Acknowledgements

I thank Simone Biondini, Torsten Bringmann and Kimmo Kainulainen for helpful discussions, Kalle Ala-Mattinen for providing numerical data from ref. [11], and the University of Jyväskylä for hospitality in September–November 2021, when this work got under way. My research was partly supported by the Swiss National Science Foundation (SNSF) under grant 200020B-188712.

A. Details of matrix elements squared

The purpose of this appendix is to list the matrix elements squared originating from the reactions shown in fig. 1. We recall that the optimal procedure is to determine the algebraic structures of would-be $1 \rightarrow 2$ and $1 \rightarrow 3$ rates, even if these are kinematically forbidden in practice. The other real processes ($2 \rightarrow 1$, $2 \rightarrow 2$, $3 \rightarrow 1$) can then be generated by crossings, whereas the IR-sensitive virtual corrections to $1 \leftrightarrow 2$ are obtained by finding the poles and residues appearing in the matrix elements squared [21].

A.1. Gauge and scalar effects

The leading-order diagram, shown in fig. 1(a), yields

$$\omega \Gamma_{1 \rightarrow 2}^{\text{real}} = \kappa^2 v^2 \text{scat}_{1 \rightarrow 2}(\tilde{\varphi}, h) , \quad (\text{A.1})$$

where $\text{scat}_{1 \rightarrow 2}$ corresponds to the notation introduced in eq. (2.4).

The next-to-leading order contributions from fig. 1(b) are suppressed by $\sim g^2$ with respect to eq. (A.1), where g^2 is a generic Standard Model coupling. As a crosscheck, we have computed them in two different ways. One goes through the usual $\sum_{\text{spins}} |\mathcal{M}|^2$, cf. eq. (2.5), keeping only physical states as external particles and recalling that the polarization sum for a massive gauge boson of mass m and four-momentum \mathcal{P} reads $\sum_{\lambda} \epsilon_{\lambda}^{\mu} \epsilon_{\lambda}^{\nu*} = -\eta^{\mu\nu} + \mathcal{P}^{\mu} \mathcal{P}^{\nu} / m^2$. The other method proceeds by computing the 2-loop self-energy of the decaying particle, and extracting its cut. A benefit of the latter approach is that it can straightforwardly be carried out in a general R_{ξ} gauge, including ghosts, and that subsequently the gauge independence of the result can be verified. Both methods yield the same results.

Re-expressing subsequently $g^2 v^2$ as a mass squared, the final expression of $\mathcal{O}(\kappa^2)$ can be put in the form

$$\begin{aligned} \omega \Gamma_{1 \rightarrow 3}^{\text{real}} \supset \kappa^2 \Bigg\{ & \text{scat}_{1 \rightarrow 3}(\tilde{\varphi}, h, h) \frac{(s_{23} + 2m_h^2)^2}{2(s_{23} - m_h^2)^2} \\ & + \text{scat}_{1 \rightarrow 3}(\tilde{\varphi}, Z^0, Z^0) \frac{(s_{23} - 2m_Z^2)^2 + 8m_Z^4}{2(s_{23} - m_h^2)^2} \\ & + \text{scat}_{1 \rightarrow 3}(\tilde{\varphi}, W^+, W^-) \frac{(s_{23} - 2m_W^2)^2 + 8m_W^4}{(s_{23} - m_h^2)^2} \Bigg\} . \end{aligned} \quad (\text{A.2})$$

Going towards the symmetric phase, so that the masses go to zero, this agrees with the first part of eq. (3.5).

As shown by the diagrams in figs. 1(b,c), there are also amplitudes that are quadratic in the coupling κ (κ is indicated by the small blob). For the matrix element squared, this produces interference terms that are cubic in κ ,

$$\omega \Gamma_{1 \rightarrow 3}^{\text{real}} \supset 2\kappa^3 v^2 \text{scat}_{1 \rightarrow 3}(\tilde{\varphi}, h, h) \frac{s_{23} + 2m_h^2}{(s_{12} - m_{\varphi}^2)(s_{23} - m_h^2)} , \quad (\text{A.3})$$

as well as quartic dependences,

$$\begin{aligned} \omega \Gamma_{1 \rightarrow 3}^{\text{real}} \supset \kappa^4 v^4 \Bigg\{ & \text{scat}_{1 \rightarrow 3}(\tilde{\varphi}, h, h) \left[\frac{1}{(s_{12} - m_{\varphi}^2)^2} + \frac{1}{(s_{12} - m_{\varphi}^2)(s_{13} - m_{\varphi}^2)} \right] \\ & + \text{scat}_{1 \rightarrow 3}(\tilde{\varphi}, \tilde{\varphi}, \tilde{\varphi}) \left[\frac{1}{2(s_{12} - m_h^2)^2} + \frac{1}{(s_{12} - m_h^2)(s_{13} - m_h^2)} \right] \Bigg\} . \end{aligned} \quad (\text{A.4})$$

Likewise, there are terms with one or two appearances of λ_φ ,

$$\omega \Gamma_{1 \rightarrow 3}^{\text{real}} \supset 6\lambda_\varphi \left\{ \frac{\kappa^2 v^2}{s_{12} - m_h^2} + \lambda_\varphi \right\} \text{scat}_{1 \rightarrow 3}(\tilde{\varphi}, \tilde{\varphi}, \tilde{\varphi}) , \quad (\text{A.5})$$

but they only contribute to kinetic equilibration. The last term differs from eq. (3.5) in that the mass of the φ -particle has changed through the Higgs mechanism.

A.2. Leptonic and hadronic effects

At low temperatures, $\pi T \ll \min\{m_w, m_h, m_\varphi\}$, the most important effects originate from fermionic channels. As long as we are in the deconfined phase ($T \gg 160$ MeV), the contributions of leptons and light quarks (at leading order in α_s) amount to

$$\begin{aligned} \omega \Gamma_{1 \rightarrow 3}^{\text{real}} \supset & \kappa^2 \sum_{\ell} \text{scat}_{1 \rightarrow 3}(\tilde{\varphi}, \ell, \bar{\ell}) \frac{2m_\ell^2(s_{23} - 4m_\ell^2)}{(s_{23} - m_h^2)^2} \\ & + \kappa^2 N_c \sum_q \text{scat}_{1 \rightarrow 3}(\tilde{\varphi}, q, \bar{q}) \frac{2m_q^2(s_{23} - 4m_q^2)}{(s_{23} - m_h^2)^2} , \end{aligned} \quad (\text{A.6})$$

where $\ell \in \{e, \mu, \tau\}$ enumerates the charged leptons, and $q \in \{u, d, s, c, b, t\}$ the quarks with $m_q \ll \max\{\pi T, m_\varphi/2\}$. Quarks heavier than this can be integrated out, yielding the higher-dimensional operator in eq. (3.4). This gives the loop-suppressed contribution

$$\omega \Gamma_{1 \rightarrow 3}^{\text{real}} \supset \frac{4\kappa^2 a_s^2 (N_c^2 - 1)}{9} \text{scat}_{1 \rightarrow 3}(\tilde{\varphi}, g, g) \frac{s_{23}^2}{(s_{23} - m_h^2)^2} , \quad (\text{A.7})$$

where $a_s \equiv \alpha_s/\pi \equiv g_3^2/(4\pi^2)$ and g stands for a gluon. If we instead go to $T \ll 160$ MeV, hadronic degrees of freedom are represented by pions. Treating them as degenerate for simplicity, we find

$$\omega \Gamma_{1 \rightarrow 3}^{\text{real}} \supset \frac{\kappa^2 (N_f^2 - 1)}{2} \text{scat}_{1 \rightarrow 3}(\tilde{\varphi}, \pi, \bar{\pi}) \frac{m_\pi^4}{(s_{23} - m_h^2)^2} , \quad (\text{A.8})$$

where $N_f = 2$ is the number of light flavours.

B. Phase space integrals for the leading-order process

We show in this appendix how the phase space integrals corresponding to the leading-order process, cf. eq. (A.1), can be carried out analytically in the non-relativistic limit $\pi T \ll m_\varphi$.

Incorporating the crossed channels and denoting the corresponding phase-space average by $\text{scat}_{1 \leftrightarrow 2}(\tilde{\varphi}, h)$ [21], the physical $\varphi\varphi \rightarrow h$ annihilation and $h \rightarrow \varphi\varphi$ pair creation rates can be represented as

$$\omega \Gamma_{1 \leftrightarrow 2}^{\text{real}} = \text{scat}_{1 \leftrightarrow 2}(\tilde{\varphi}, h) \Theta_{1 \leftrightarrow 2} , \quad \Theta_{1 \leftrightarrow 2} \equiv \kappa^2 v^2 . \quad (\text{B.1})$$

We perform the phase-space integrals in the plasma rest frame, with $(\omega \equiv \sqrt{k^2 + m_\varphi^2}, \mathbf{k})$ denoting the four-momentum of one of the singlet scalars. For a momentum-independent $\Theta_{1 \leftrightarrow 2}$ and denoting $\beta \equiv 1/T$, this yields [33]

$$\begin{aligned} \text{scat}_{1 \leftrightarrow 2}(\tilde{\varphi}, h) &\stackrel{m_\varphi < m_h/2}{=} \frac{T}{16\pi k} \ln \left\{ \frac{1 - e^{-\beta\epsilon_h^-}}{1 - e^{-\beta\epsilon_h^+}} \frac{1 - e^{-\beta(\epsilon_h^+ - \omega)}}{1 - e^{-\beta(\epsilon_h^- - \omega)}} \right\}_{\epsilon_h^\pm = \frac{m_h^2}{2m_\varphi^2} \left(\omega \pm k \sqrt{1 - \frac{4m_\varphi^2}{m_h^2}} \right)} \\ &\stackrel{\pi T \ll m_\varphi}{\approx} \frac{T}{16\pi k} \left\{ e^{-\beta(\epsilon_h^- - \omega)} - e^{-\beta(\epsilon_h^+ - \omega)} \right\}, \end{aligned} \quad (\text{B.2})$$

where ϵ_h^\pm denote the maximal and minimal energies of the Higgs boson (originating from different angular configurations) when the momentum of one of the φ particles has been fixed, and $\epsilon_h^\pm - \omega$ are those of the co-annihilation partner. Expanding the exponentials in eq. (B.2) in $k/\omega < 1$ and employing ω as the integration variable, so that $k = \sqrt{\omega^2 - m_\varphi^2}$, momentum averaging yields

$$\begin{aligned} \langle \Gamma_{1 \leftrightarrow 2}^{\text{real}} \rangle &\stackrel{\pi T \ll m_\varphi}{\approx} \frac{1}{n_{\text{eq}}} \int_0^\infty \frac{dk k^2}{2\pi^2} \frac{e^{-\beta\omega}}{\omega} \text{scat}_{1 \leftrightarrow 2}(\tilde{\varphi}, h) \Theta_{1 \leftrightarrow 2} \\ &\stackrel{(\text{B.2})}{\approx} \stackrel{(\text{B.4})}{=} \frac{m_\varphi \kappa^2 v^2 T}{16\pi^3 n_{\text{eq}}} \sqrt{1 - \frac{4m_\varphi^2}{m_h^2}} \sum_{n=0}^\infty \frac{1}{n!} \left(\frac{m_h^2 - 4m_\varphi^2}{4m_\varphi T} \right)^n K_{1+n} \left(\frac{m_h^2}{2m_\varphi T} \right) \\ &\stackrel{(\text{B.5})}{=} \frac{\kappa^2 v^2 T}{32\pi^3 n_{\text{eq}}} \sqrt{m_h^2 - 4m_\varphi^2} K_1 \left(\frac{m_h}{T} \right), \end{aligned} \quad (\text{B.3})$$

where K_ν is a modified Bessel function, and we made use of the integral representations

$$K_\nu(z) = \frac{\Gamma(\frac{1}{2})}{\Gamma(\nu + \frac{1}{2})} \left(\frac{z}{2} \right)^\nu \int_1^\infty dt e^{-zt} (t^2 - 1)^{\nu - \frac{1}{2}} \quad (\text{B.4})$$

$$= \frac{1}{2} \left(\frac{z}{2} \right)^\nu \int_0^\infty \frac{dt}{t^{\nu+1}} \exp \left(-t - \frac{z^2}{4t} \right). \quad (\text{B.5})$$

The equilibrium density can be written as

$$n_{\text{eq}} = \int_0^\infty \frac{dk k^2}{2\pi^2} f_{\text{B}}(\omega) \stackrel{\pi T \ll m_\varphi}{\approx} \stackrel{(\text{B.4})}{=} \frac{m_\varphi^2 T}{2\pi^2} K_2 \left(\frac{m_\varphi}{T} \right), \quad (\text{B.6})$$

where we again took ω as an integration variable. The momentum-averaged cross section from eq. (2.23) becomes

$$\langle \sigma v_{\text{rel}} \rangle_{1 \leftrightarrow 2} \equiv \frac{\langle \Gamma_{1 \leftrightarrow 2}^{\text{real}} \rangle}{n_{\text{eq}}} \stackrel{m_\varphi < m_h/2}{\approx} \stackrel{\pi T \ll m_\varphi}{=} \frac{\pi \kappa^2 v^2 \sqrt{m_h^2 - 4m_\varphi^2} K_1 \left(\frac{m_h}{T} \right)}{8m_\varphi^4 T K_2^2 \left(\frac{m_\varphi}{T} \right)}. \quad (\text{B.7})$$

References

- [1] K. Griest and D. Seckel, *Three exceptions in the calculation of relic abundances*, Phys. Rev. D 43 (1991) 3191.
- [2] P. Gondolo and G. Gelmini, *Cosmic abundances of stable particles: Improved analysis*, Nucl. Phys. B 360 (1991) 145.
- [3] V. Silveira and A. Zee, *Scalar Phantoms*, Phys. Lett. B 161 (1985) 136.
- [4] J. McDonald, *Gauge singlet scalars as cold dark matter*, Phys. Rev. D 50 (1994) 3637 [hep-ph/0702143].
- [5] C.P. Burgess, M. Pospelov and T. ter Veldhuis, *The Minimal Model of nonbaryonic dark matter: a singlet scalar*, Nucl. Phys. B 619 (2001) 709 [hep-ph/0011335].
- [6] J.M. Cline, K. Kainulainen, P. Scott and C. Weniger, *Update on scalar singlet dark matter*, Phys. Rev. D 88 (2013) 055025; *ibid.* 92 (2015) 039906 (E) [1306.4710].
- [7] J. Heisig, M. Krämer, E. Madge and A. Mück, *Probing Higgs-portal dark matter with vector-boson fusion*, JHEP 03 (2020) 183 [1912.08472].
- [8] T. Binder, T. Bringmann, M. Gustafsson and A. Hryczuk, *Early kinetic decoupling of dark matter: when the standard way of calculating the thermal relic density fails*, Phys. Rev. D 96 (2017) 115010; *ibid.* 101 (2020) 099901 (E) [1706.07433].
- [9] K. Ala-Mattinen and K. Kainulainen, *Precision calculations of dark matter relic abundance*, JCAP 09 (2020) 040 [1912.02870].
- [10] T. Binder, T. Bringmann, M. Gustafsson and A. Hryczuk, *Dark matter relic abundance beyond kinetic equilibrium*, Eur. Phys. J. C 81 (2021) 577 [2103.01944].
- [11] K. Ala-Mattinen, M. Heikinheimo, K. Kainulainen and K. Tuominen, *Momentum distributions of cosmic relics: Improved analysis*, Phys. Rev. D 105 (2022) 123005 [2201.06456].
- [12] T. Abe, *Early kinetic decoupling and a pseudo-Nambu-Goldstone dark matter model*, Phys. Rev. D 104 (2021) 035025 [2106.01956].
- [13] Y. Du, F. Huang, H.-L. Li, Y.-Z. Li and J.-H. Yu, *Revisiting dark matter freeze-in and freeze-out through phase-space distribution*, JCAP 04 (2022) 012 [2111.01267].
- [14] T. Bringmann, S. Heeba, F. Kahlhoefer and K. Vangsnes, *Freezing-in a hot bath: resonances, medium effects and phase transitions*, JHEP 02 (2022) 110 [2111.14871].
- [15] J. Ghiglieri and U.A. Wiedemann, *Thermal width of the Higgs boson in hot QCD matter*, Phys. Rev. D 99 (2019) 054002 [1901.04503].
- [16] M. Beneke, A.P. Chapovsky, A. Signer and G. Zanderighi, *Effective theory calculation of resonant high-energy scattering*, Nucl. Phys. B 686 (2004) 205 [hep-ph/0401002].
- [17] T. Kinoshita, *Mass Singularities of Feynman Amplitudes*, J. Math. Phys. 3 (1962) 650.
- [18] T.D. Lee and M. Nauenberg, *Degenerate Systems and Mass Singularities*, Phys. Rev. 133 (1964) B1549.

- [19] M. Beneke, F. Dighera and A. Hryczuk, *Relic density computations at NLO: infrared finiteness and thermal correction*, JHEP 10 (2014) 045; *ibid.* 07 (2016) 106 (E) [1409.3049].
- [20] D. Bödeker, M. Sangel and M. Wörmann, *Equilibration, particle production, and self-energy*, Phys. Rev. D 93 (2016) 045028 [1510.06742].
- [21] G. Jackson and M. Laine, *Efficient numerical integration of thermal interaction rates*, JHEP 09 (2021) 125 [2107.07132].
- [22] D. Bödeker and M. Laine, *Heavy quark chemical equilibration rate as a transport coefficient*, JHEP 07 (2012) 130 [1205.4987].
- [23] J. Bernstein, L.S. Brown and G. Feinberg, *Cosmological heavy-neutrino problem*, Phys. Rev. D 32 (1985) 3261.
- [24] M. D’Onofrio and K. Rummukainen, *Standard Model cross-over on the lattice*, Phys. Rev. D 93 (2016) 025003 [1508.07161].
- [25] T. Inami, T. Kubota and Y. Okada, *Effective gauge theory and the effect of heavy quarks in Higgs boson decays*, Z. Phys. C 18 (1983) 69.
- [26] T. Asaka, M. Laine and M. Shaposhnikov, *Lightest sterile neutrino abundance within the ν MSM*, JHEP 01 (2007) 091; *ibid.* 02 (2015) 028 (E) [hep-ph/0612182].
- [27] M. Laine and Y. Schröder, *Quark mass thresholds in QCD thermodynamics*, Phys. Rev. D 73 (2006) 085009 [hep-ph/0603048].
- [28] M. Laine and M. Meyer, *Standard Model thermodynamics across the electroweak crossover*, JCAP 07 (2015) 035 [1503.04935].
- [29] S. Biondini and J. Ghiglieri, *Freeze-in produced dark matter in the ultra-relativistic regime*, JCAP 03 (2021) 075 [2012.09083].
- [30] S. Caron-Huot and G.D. Moore, *Heavy quark diffusion in perturbative QCD at next-to-leading order*, Phys. Rev. Lett. 100 (2008) 052301 [0708.4232].
- [31] S. Caron-Huot, M. Laine and G.D. Moore, *A way to estimate the heavy quark thermalization rate from the lattice*, JHEP 04 (2009) 053 [0901.1195].
- [32] G.D. Moore and D. Teaney, *How much do heavy quarks thermalize in a heavy ion collision?*, Phys. Rev. C 71 (2005) 064904 [hep-ph/0412346].
- [33] J. Ghiglieri and M. Laine, *Smooth interpolation between thermal Born and LPM rates*, JHEP 01 (2022) 173 [2110.07149].